Disruption of *PPT1* or *PPT2* causes neuronal ceroid lipofuscinosis in knockout mice

Praveena Gupta*, Abigail A. Soyombo*, Armita Atashband*, Krystyna E. Wisniewski†‡, John M. Shelton§, James A. Richardson¶, Robert E. Hammer‖, and Sandra L. Hofmann*††**

*The Hamon Center for Therapeutic Oncology Research and §Division of Cardiology, Department of Internal Medicine, Departments of ¶Pathology and ‖Biochemistry, and the **Howard Hughes Medical Institute, University of Texas Southwestern Medical Center, Dallas, TX 75390; †Department of Pathological Neurobiology, New York State Institute for Basic Research in Developmental Disabilities, Staten Island, NY 10314; and ‡State University of New York/Health Science Center, Brooklyn, NY 11203

Edited by Joseph L. Goldstein, University of Texas Southwestern Medical Center, Dallas, TX, and approved October 12, 2001 (received for review September 14, 2001)

***PPT1* and *PPT2* encode two lysosomal thioesterases that catalyze the hydrolysis of long chain fatty acyl CoAs. In addition to this function, PPT1 (palmitoyl-protein thioesterase 1) hydrolyzes fatty acids from modified cysteine residues in proteins that are undergoing degradation in the lysosome. PPT1 deficiency in humans causes a neurodegenerative disorder, infantile neuronal ceroid lipofuscinosis (also known as infantile Batten disease). In the current work, we engineered disruptions in the PPT1 and PPT2 genes to create ''knockout'' mice that were deficient in either enzyme. Both lines of mice were viable and fertile. However, both lines developed spasticity (a ''clasping'' phenotype) at a median age of 21 wk and 29 wk, respectively. Motor abnormalities progressed in the PPT1 knockout mice, leading to death by 10 mo of age. In contrast, the majority of PPT2 mice were alive at 12 mo. Myoclonic jerking and seizures were prominent in the PPT1 mice. Autofluorescent storage material was striking throughout the brains of both strains of mice. Neuronal loss and apoptosis were particularly prominent in PPT1-deficient brains. These studies provide a mouse model for infantile neuronal ceroid lipofuscinosis and further suggest that PPT2 serves a role in the brain that is not carried out by PPT1.**

The neuronal ceroid lipofuscinoses (NCLs) are a distinct class of lysosomal storage disorders with a worldwide prevalence of 1:12,500 (1). The pathological hallmark of the NCLs is the accumulation of autofluorescent storage material in the brain and other tissues, associated with progressive psychomotor retardation, visual failure, and seizures. Up to eight forms of NCL are now recognized (designated NCL-1 through NCL-8) and are caused by autosomal recessive mutations in genes designated CLN1 through CLN8, respectively (2). Five of these genes have been cloned, a sixth chromosomal locus has been well characterized (CLN6), and two others (CLN4 and CLN7) have clinical or other distinctive features suggesting that they represent distinct genes as well.

The most severe form of NCL, infantile NCL (NCL-1) is caused by deficiency in a lysosomal thioesterase (palmitoyl-protein thioesterase 1, or PPT1) whose function is to remove long-chain fatty acids from modified cysteine residues in proteins (3). This function is suggested by its enzymatic activity and the observation that fatty acid esters of cysteine accumulate in cells derived from patients with the disorder (4). A second enzyme, PPT2, shares an 18% amino acid homology with PPT1 (5). Like PPT1, PPT2 hydrolyzes long-chain fatty acyl CoAs, but it does not hydrolyze the fatty acyl-cysteine thioesters that accumulate in PPT1-deficient cells (5).

In the current study, we have created mouse mutants with disrupted *PPT1* and *PPT2* genes. We find that disruption of either gene causes neuronal ceroid lipofuscinosis in mice.

Materials and Methods

Generation of PPT1 and PPT2 Knockout Mice. The *PPT1*-targeting vector (Fig. 1*A*) was based on the plasmid pNotI-Pme-Srf (6), which contains a pPolII-neobPA cassette and two copies of the herpes simplex virus thymidine-kinase (*TK*) gene (7). A long arm (consisting of a 9-kb fragment spanning exon 4 through a portion of exon 9 of the *PPT1* gene) was amplified by using isogenic 129S6/SvEvTac murine genomic DNA and the following primer pairs: 5′-ATAAGAATGCGGCCGCAGAGAGTTCTCA-CATCTGCGACTTCATCAGGAA-3′ and 5′-ATAAGAAT-GCGGCCGCCAATCCACTAGCTTTCCTGCTTTGTC-CATTTTCTTTAG-3′. Sequences for the primer pairs were derived from GenBank (accession nos. AF071025 and AF087568). An in-frame termination codon was placed at the 3′ end of the long arm, and the fragment was cloned into the *Not*I site of the vector. A 1-kb short arm consisting of exon 9 sequences was amplified with primers 5′-CCGCTCGAGTGC-TATCACCATATGGTGTT-3′ and 5′-CCGCTCGAGGGT-GAATTCTGTGGTGCTAA-3′ and was subcloned into the *Xho*I site of the vector. The construct was linearized with *Pme*I before electroporation. The *PPT2* targeting vector (Fig. 2*A*) consisted of the following: two copies of the herpes simplex virus thymidine-kinase (*TK*) gene on a *Xho*I/*Pme*I fragment derived from pNotI-Pme-Srf (6); a short arm consisting of a 1.0-kb *Bam*HI/*Xba*I fragment corresponding to sequences from exon 1 to a part of exon 3 of mouse *PPT2*, amplified by PCR by using the following primer pairs: 5′-CATCCGGCTAAATG-GATCGCTCTG-3′ and 5′-TCACACCACAGTCCCGGTGT-GTGT-3′ on isogenic 129S6/SvEvTac genomic DNA; a 1.8-kb *Bam*HI/*Xba*I fragment containing an in-frame termination codon and the neomycin resistance cassette derived from plasmid pFloxΔ*Eco*RI (8); and a long arm consisting of a 9-kb fragment with sequences from intron 4 to a part of exon 9, amplified by PCR by using primers 5′-GTCTGAGCTTGAC-CCTTATCTAAGGCCTACTTT-3′ and 5′-GAATCTCGAA-GATACACCTTCGAGGTGGGCCGA-3′. Primer sequences were derived from GenBank mouse genomic sequences (AF030001). The final targeting construct was propagated in the vector pGEM-11Zf(+) (Promega) and linearized with *Sfi*I. Linearized vectors were introduced into murine SM-1 embryonic stem cells derived from the 129S6/SvEvTac strain by electroporation, and subsequent cloning of homologous recombinant colonies was carried out as described (9). Targeting efficiencies were 2.2% and 0.4% for *PPT1* and *PPT2* vectors, respectively. Two positive clones derived from each targeting construct were expanded and injected into C57BL/6J blastocysts. High-percentage male chimeras from two independent embryonic

This paper was submitted directly (Track II) to the PNAS office.

Abbreviations: GROD, granular osmiophilic deposits; PPT, palmitoyl protein thioesterase; NCL, neuronal ceroid lipofuscinosis.

††To whom reprint requests should be addressed. E-mail: Sandra.Hofmann@utsouthwestern.edu.

The publication costs of this article were defrayed in part by page charge payment. This article must therefore be hereby marked "*advertisement*" in accordance with 18 U.S.C. §1734 solely to indicate this fact.

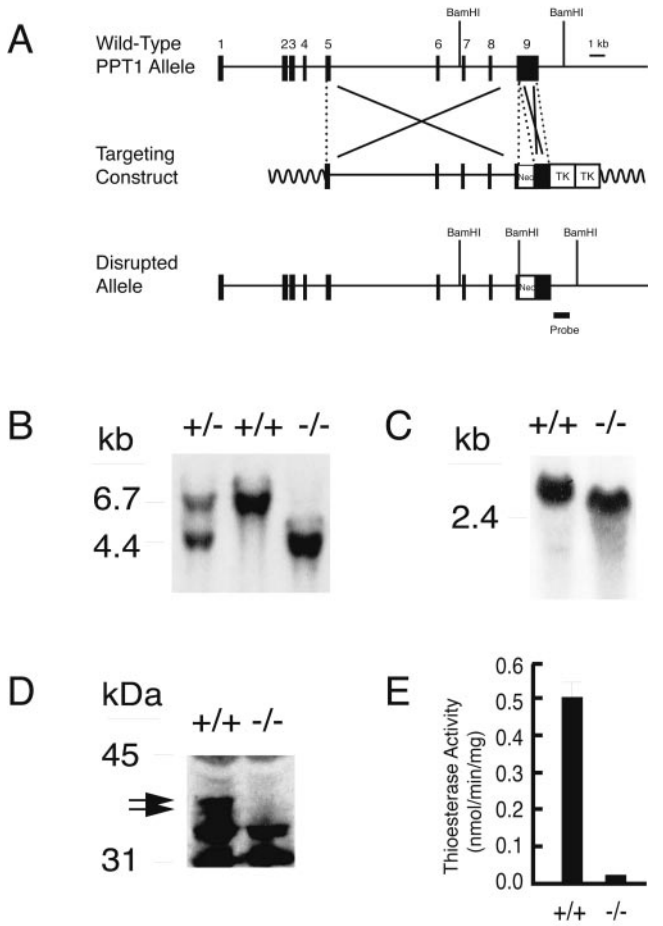

Fig. 1. Targeted disruption of the *PPT1* gene. (*A*) The structure of the endogenous mouse *PPT1* gene, the targeting construct, and the disrupted allele. The position of a 600-bp probe used for Southern blotting is shown. (*B*) Southern blot analysis of *Bam*HI-digested genomic DNA. A 6.7-kb fragment is detected in wild-type animals and a 4.4-kb fragment is detected in *PPT1* knockout mice. (*C*) An RNA blot of total kidney RNA (20 μg) of wild-type and *PPT1* ($-/-$) littermates hybridized with a 300-bp mouse *PPT1* coding region probe. (*D*) Immunoblotting of brain extract by using an anti-rat PPT1 Ab. An $\approx$37-kDa doublet (arrows) corresponding to glycosylated PPT1 is absent from *PPT1* ($-/-$) mice. Bands appearing in both wild-type and knockout were deemed nonspecific because they were also visualized by using preimmune serum (data not shown). (*E*) PPT1 activity in wild-type and *PPT1* ($-/-$) brain extracts.

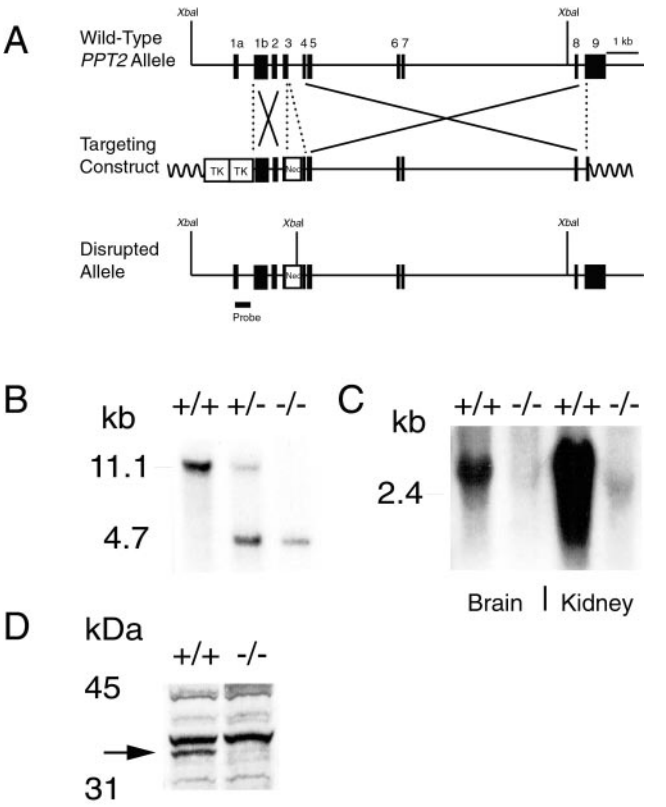

Fig. 2. Targeted disruption of the *PPT2* gene. (*A*) The structure of the endogenous mouse *PPT2* gene, the targeting construct, and the disrupted allele. The position of a 507-bp probe that was used for Southern blotting is shown. (*B*) Southern blot analysis of *Xba*I-digested genomic DNA. An 11.1-kb band is detected in wild-type and a 4.7-kb fragment is detected in *PPT2* knockout mice. (*C*) RNA blotting of total brain and kidney RNA (20 μg) hybridized with a 300-bp mouse *PPT2* coding region probe. (*D*) PPT2 immunoblotting of kidney extracts from wild-type and *PPT2* knockout mice. A 35-kDa band, corresponding to deglycosylated PPT2, is absent from the *PPT2* knockout mice. Bands appearing in both wild-type and knockout were deemed nonspecific because they were also visualized by using preimmune serum (data not shown).

stem cell clones for each knockout were crossed with female C57BL/6J mice to generate two lines of animals carrying the disrupted *PPT1* or *PPT2* allele (a total of four lines). No phenotypic differences were observed between mice derived from each of the two independent embryonic stem cell lines for each knockout. Phenotypic characterization was carried out in the mixed C57BL/6J $\times$ 129S6/SvEvTac animals.

RNA and Enzyme Assays. RNA blotting was performed as described (10). Immunoblotting was performed by using rabbit anti-rat PPT1 (11) or an anti-mouse PPT2 peptide Ab corresponding to amino acid residues Cys-249–Thr-268 raised in chickens (10). Immunoreactive bands were detected by enhanced chemiluminescence (ECL, Amersham Pharmacia). PPT1 enzymatic activity was detected by using 4-methylumbelliferyl-6-thiopalmitoyl-β-D-glucoside as the substrate (12). Assays were performed on brain homogenates after preincubation with 4 mM PMSF for 20 min at 37°C to reduce background thioesterase activity.

Behavioral Studies. A tail suspension test was performed by grasping the tail and holding the mouse $\approx$1 foot from a solid surface for 30 sec (13). The test was considered positive if all four limbs came to the midline and remained in place for several seconds. Frequency of myoclonic jerks was observed by placing mice individually in a clean cage in a quiet room for a 5-min period. Testing was done during the daylight cycle by a blinded observer. No phenotypic abnormalities were seen in heterozygous mice. Controls in behavioral studies included both wild-type and heterozygous littermates.

Histological Studies. Radioisotopic RNA *in situ* hybridizations were performed as described (14). RNA probes were made from templates derived by reverse transcription–PCR from mouse brain cDNA and corresponded to nucleotides 541–840 (GenBank accession no. AF070025) and 418–710 (GenBank accession no. NM_019441) of the mouse PPT1 (15) and PPT2 cDNAs, respectively. Autoradiographic exposure was for 28 days. Serial sections of brain were deparaffinized and stained with routine hematoxylin and eosin for pathological evaluation, left unstained, and coverslipped with Vectashield (Vector Labs, Burlingame, CA) for evaluation of autofluorescent pigment (excitation, 470 $\pm$ 20 nm, emission, 525 $\pm$ 25 nm), or subjected to terminal deoxynucleotidyltransferase-mediated dUTP end la-

beling by using a commercial reagent kit (Apoptosis Detection System, Fluorescein, Promega catalog no. G3250). Fixation, permeabilization, and staining runs were carried out in exact parallel to ensure comparative significance between groups (16). Electron microscopy was performed as described (17).

Results

Gene Disruptions. Fig. 1 illustrates the *PPT1* gene targeting strategy and resulting PPT1 deficiency in knockout mice. A portion of exon 9 was replaced by a neomycin resistance cassette containing an in-frame stop codon, resulting in premature termination of the PPT1 polypeptide at amino acid Val-281, which is upstream of an essential catalytic amino acid (His-289) (Fig. 1*A*). Southern blotting of genomic tail DNA (Fig. 1*B*) revealed the expected *Bam*HI fragments of 6.7 kb (wild-type) and 4.4 kb (knockout). RNA blotting of brain tissue (Fig. 1*C*) and other tissues (not shown) revealed normal amounts of a truncated PPT1 mRNA. However, a complete absence of the characteristic PPT1 doublet at 37 kDa on immunoblots (Fig. 1*D*), coupled with background levels of PPT1 enzymatic activity (Fig. 1*E*), confirmed the successful disruption of *PPT1* in these animals.

PPT2 was disrupted by using a similar strategy (Fig. 2*A*), with the exception that the neomycin resistance gene was flanked by *loxP* sites and inserted into exon 3 of *PPT2* (the *loxP* sites were not used in the current study). Homozygotes carrying the targeted allele showed the expected 4.7-kb *Xba*I fragment on Southern blotting of genomic DNA (Fig. 2*B*) and an absence of PPT2-specific message by RNA blotting of brain and kidney (Fig. 2*C*). The absence of PPT2 protein was confirmed by immunoblotting of PNGaseF-treated kidney extracts from wild-type and knockout mice (Fig. 2*D*).

Phenotypes. Both PPT1- and PPT2-deficient mice were healthy at birth. Beginning as early as 50 days of age, PPT1-deficient mice showed a strongly abnormal clasping behavior in the tail suspension test (Fig. 3*A*). This neurological abnormality developed in 50% of mice by 5 mo and 100% of the animals by 8 mo of age. Interestingly, only 50% of PPT2-deficient mice showed clasping behavior by 8 mo.

In addition to the clasping abnormality, PPT1-deficient mice at 4–5 mo began to show a lack of grooming, followed by a progressive gait abnormality including lowering of the pelvis, splayed hind limbs, hunched posture, and a side-to-side wobbling gait, which eventually progressed to hind-limb paralysis. Aggressive behavior, manifested by frequent bite wounds and consequent dermatitis, was a problem in the colony. Older animals were killed as they became visibly ill. Mortality reached 50% among the PPT1 mice by 7 mo and few mice survived past 10 mo (Fig. 3*B*). At 10 mo, PPT2 mice showed no gross motor abnormalities aside from spasticity. Mortality was slightly increased (80% survival at 10 mo).

Frequent myoclonic jerks and seizures were observed in the PPT1-deficient mice beginning at ≈3–4 mo of age. The myoclonic jerks were brief, upper body contractions (resembling a violent sneeze) that usually interrupted the forward progression of the animal. Fig. 3*C* shows the number of myoclonic jerks observed in a 5-min period of observation for 12 homozygotes and 12 controls at 6 mo of age. Ten of 12 PPT1-deficient mice had an average of seven jerks per 5 min (range 5 to 15), whereas such jerks were very infrequently scored in control animals by a blinded observer. In addition, lightning-like hind limb seizures that propelled the mice several feet into the air were also seen ("popcorn" seizures). Generalized tonic-clonic convulsions were occasionally observed during routine handling, lasted 1–3 min, and resolved spontaneously without noticeable sequelae.

The assessment of visual changes in the mice was inconclusive. PPT1-deficient mice routinely failed a "visual cliff" test at 7 mo of age; however, it was unclear whether this abnormality was caused by decreased vision or concurrent sensory, motor, and/or cognitive abnormalities. Electroretinograms were markedly diminished, but conclusions were compromised by the poor vision and electroretinography of the wild-type background strain (C57BL/6J). Definitive studies await the availability of *PPT1* and *PPT2* knockouts on an appropriate high-vision background strain (such as 129SvEv).

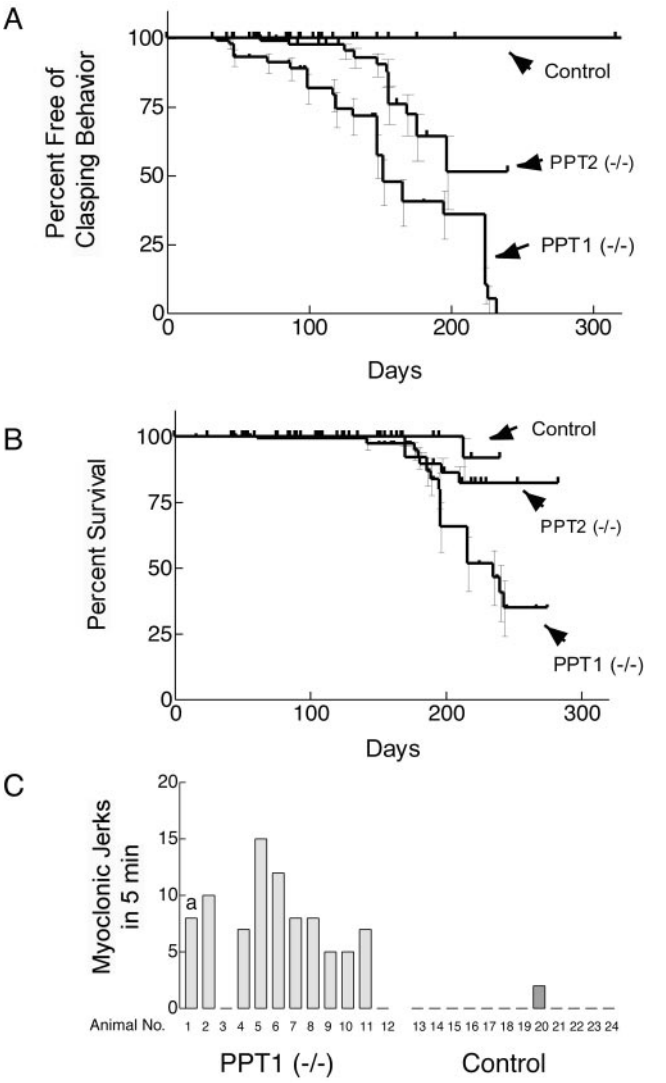

Fig. 3. Neurological abnormalities and decreased survival in PPT1 and PPT2 knockout mice. (*A*) Kaplan–Meier analysis of clasping abnormality in control, PPT1-deficient, and PPT2-deficient mice ($n = 58$, 70, and 96, respectively). The curves are significantly different from each other at a level of $P < 0.0001$ (two-tailed Mantel–Haenszel log rank test). (*B*) Kaplan–Meier survival curve of control, PPT1-deficient, and PPT2-deficient mice ($n = 72$, 129, and 160, respectively). Survival curves were statistically different from each other ($P < 0.01$). (*C*) Myoclonus in PPT1 knockout mice. Twelve *PPT1* (−/−) and 12 wild-type mice at 6 mo of age were observed individually for a 5-min period and the number of myoclonic jerks was recorded. a, A spontaneous generalized tonic-clonic seizure lasting 1 min occurred in one control mouse during the 5-min observation period.

Histological Studies. In normal mice, *PPT1* and *PPT2* showed distinctive expression patterns in the brain (Fig. 4), as assessed by RNA *in situ* hybridization. *PPT1* expression was dramatic in the Purkinje cells of the cerebellum, in the thalamus and

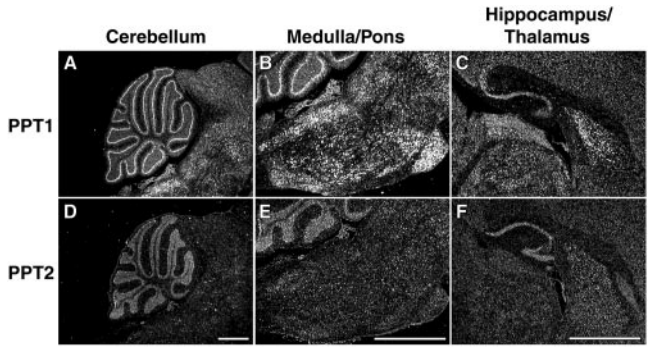

Fig. 4. PPT1 and PPT2 RNA *in situ* hybridization of sagittal sections of mouse brain. A strong PPT1 signal is seen in the Purkinje neurons of cerebellum (*A*) in the pontine and medullar nuclei of the hindbrain (*B*) and in the thalamus, hippocampus, and dentate gyrus of the forebrain (*C*). PPT2 expression was prominent in the granular layer of the cerebellum (*D*) and showed moderate expression in the pons (*E*), hippocampus, and dentate gyrus (*F*). (Bar, 1 mm.)

hippocampus, as well as in the pons and various nuclei of the medulla (Fig. 4 *A–C*). In contrast, *PPT2* expression (Fig. 4 *D–F*) was more diffuse throughout the brain and its expression level lower as compared to *PPT1*, a finding that is supported by previous work (18). *PPT2* expression in the Purkinje cells was similar to that in the granular layer, with the result that the dramatic Purkinje cell definition seen for *PPT1* was lost. Diffuse *PPT2* staining was seen throughout the medulla and pons, with scattered localized areas of signal in various nuclei of the hindbrain.

On gross pathological examination, the brains of PPT1-deficient mice were smaller and more yellow as compared to normal mice (data not shown). The calvaria were thickened and noticeably more difficult to open in older diseased animals. As compared to normal controls, markedly increased autofluorescence was noted at 4 wk of age (the earliest time examined) and florid autofluorescence was observed throughout the brains of 5-mo-old mice (Fig. 5 *Top*). Autofluorescent deposits, consisting of granular spheroid structures resembling tiny golden droplets, occupied peripheral sites around the nucleus. The smaller granules coalesced to form larger aggregates in older neurons, filling much of the cytoplasm. Storage material was detected in glial cells as well. At 5 mo, widespread storage was found throughout the cerebral cortex, Purkinje and granular layers of the cerebellum, hippocampus, thalamus and hypothalamus, dentate nucleus, pons, and some regions of the medulla (Fig. 5 *Top*). Note that in the cerebellum, the Purkinje cells are clearly outlined in a pattern similar to that of the PPT1 mRNA expression. Moderate amounts of autofluorescent storage material were seen throughout the brains of 10-mo-old PPT2-deficient mice, especially in the deeper nuclei of the cerebral cortex, hippocampus, and pons, but at 10 mo (the latest time examined) the overall intensity was less than that seen in 5-mo-old PPT1-deficient mice (Fig. 5 *Middle*). The highest accumulation of autofluorescent storage material in the PPT2-deficient brain occurred in the pontine region, which was also an area with a high level of PPT2 mRNA expression. The Purkinje layer of the cerebellum showed scant autofluorescence in PPT2-deficient mice as compared to PPT1 knockout mice, which is consistent with the modest PPT2 expression in the Purkinje layer as compared to other areas of the brain. Thus, the pattern of abnormal autofluorescent storage material in PPT1- and PPT2-deficient brain roughly paralleled the expression pattern of the two enzymes in the normal mice seen in Fig. 4.

In infantile NCL, the autofluorescent storage material has a characteristic ultrastructure when examined by electron microscopy, termed granular osmiophilic deposits (GROD). In the PPT1-deficient mice, neuronal GROD were readily identified (Fig. 6) and were indistinguishable from human GROD seen in infantile neuronal ceroid lipofuscinosis (17). In contrast, ultrastructural examination of the oldest available PPT2-deficient mice (10 mo) was inconclusive.

Pathological changes in the brains of PPT1-deficient mice

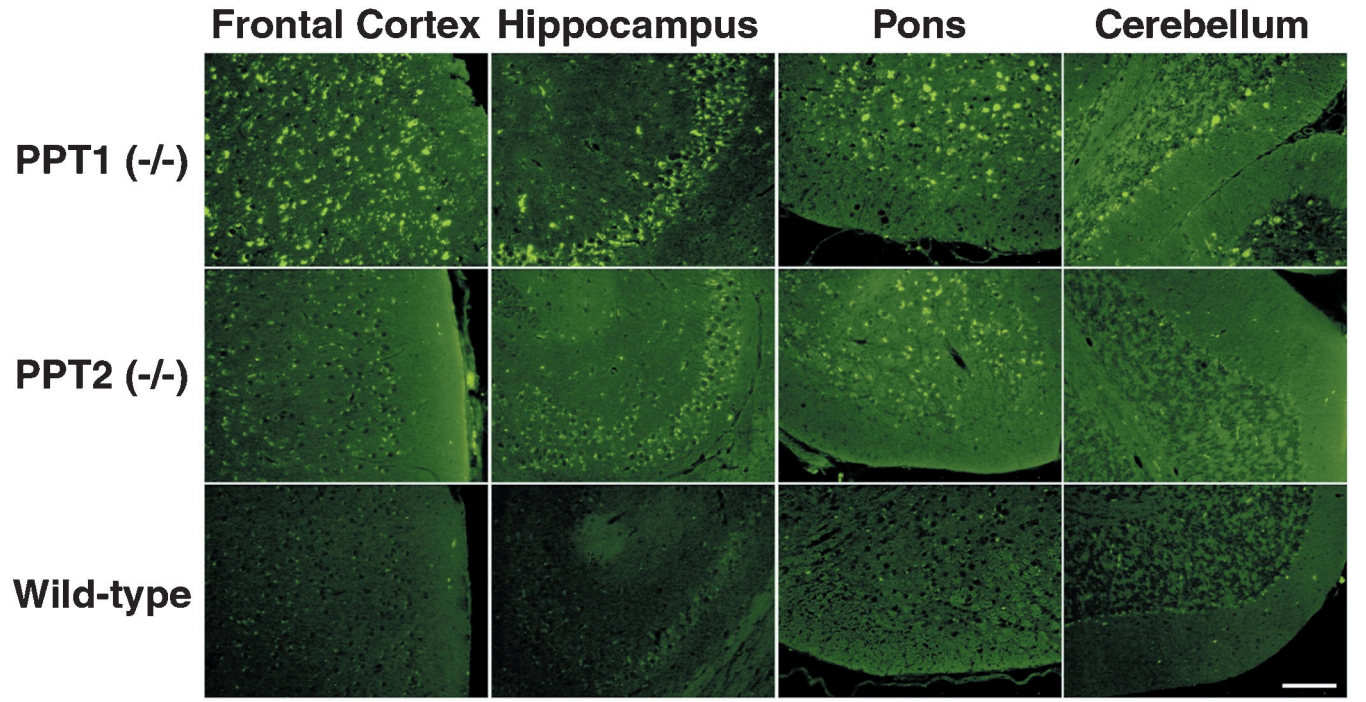

Fig. 5. Autofluorescent storage material in *PPT1* and *PPT2* knockout brain. (*Top*) brain regions as indicated from a 6-mo-old *PPT1* knockout mouse. (*Middle*) Corresponding regions from a 10-mo-old *PPT2* knockout mouse. (*Bottom*) Ten-mo-old wild-type mouse. (Bar, 100 μm.)

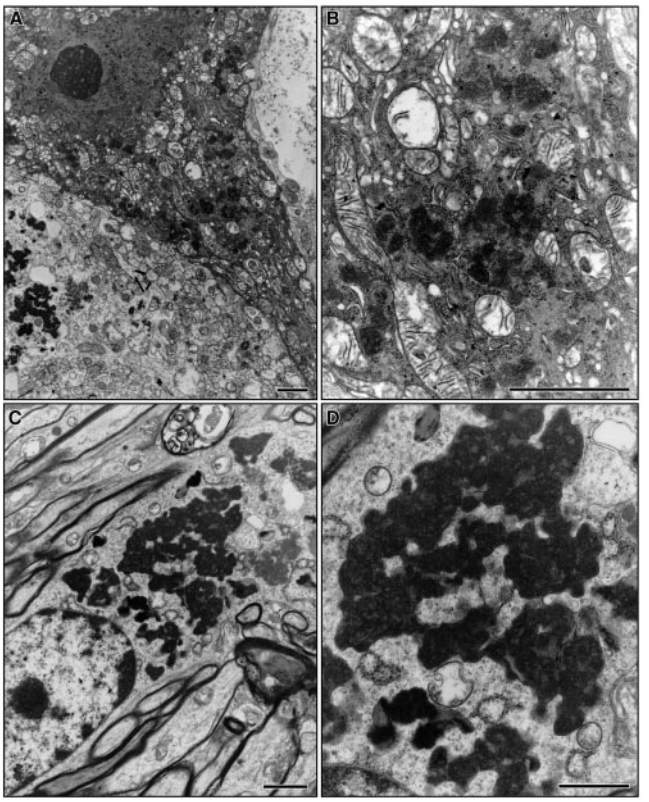

Fig. 6. Ultrastructure of granular osmiophilic deposits in brain of PPT1 knockout mice by electron microscopy. (*A* and *B*) Purkinje neuron. (*C* and *D*) Cortical neuron. (Bar, 100 nm.)

were obvious (Fig. 7). For example, the hippocampus was thinned and many neurons showed ballooning degeneration (Fig. 7*A*, large arrows) and apoptotic nuclear fragments (small arrows). Similar changes were seen in the cerebral cortex (not shown). A comparison of the Purkinje layer in PPT-deficient and wild-type mice (Fig. 7, compare *B* and *D*) show loss of continuity,

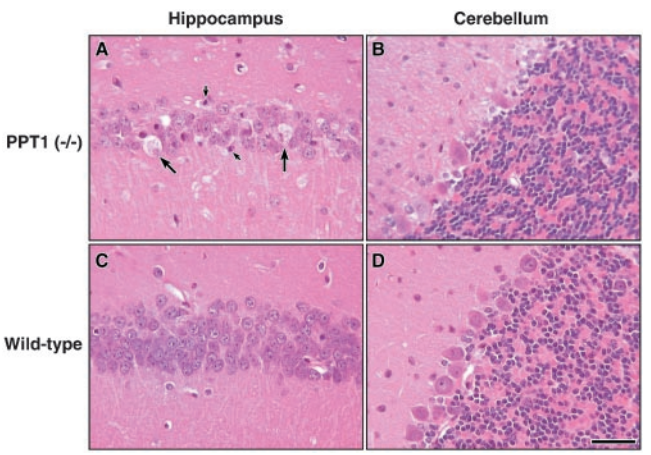

Fig. 7. Neuronal loss in PPT1 knockout mouse brains. Hematoxylin- and eosin-stained sagittal brain sections from a 6-mo-old PPT1 knockout and age-matched wild-type mouse. (*A*) PPT1−/− hippocampus showing ballooning degeneration and loss of neurons. Large arrows denote ballooning of neurons; small arrows show neuronal apoptotic bodies. (*B*) PPT1−/− Purkinje neurons in the cerebellum show neuronal loss, resulting in a discontinuous Purkinje layer. (*C*) Wild-type hippocampal region. (D) Wild-type Purkinje neurons of the cerebellum. (Bar, 40 μm.)

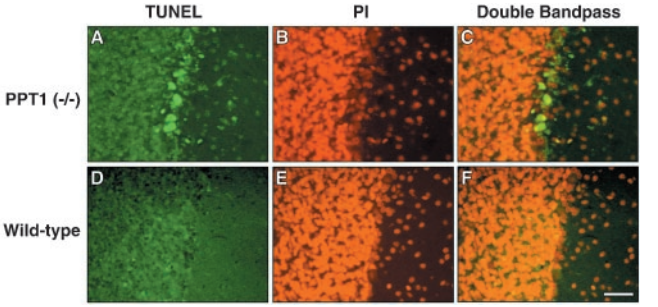

Fig. 8. Apoptotic neurons in the Purkinje layer of the cerebellum. Photomicrographs of representative sections from a 6-mo-old PPT1 knockout and wild-type mouse. (*A*) Terminal deoxynucleotidyltransferase-mediated dUTP end labeling (fluorescein, in green) performed on Purkinje neurons from a 6-mo-old PPT1 knockout (*B*) Propidium iodide nuclear staining of same region. (*C*) Overlapped images show apoptotic neurons in yellow. (*D–F*) Corresponding regions in a wild-type brain stained similarly. (Bar, 40 μm.)

with obvious Purkinje cell dropout and gliosis. Many of the remaining neurons in the affected Purkinje layer showed nuclear labeling by using a terminal deoxynucleotidyltransferase-mediated UTP end labeling assay (Fig. 8), indicating apoptosis as the mechanism of cell death in this neuronal population.

Gross pathological and histological examination of PPT2-deficient mice at 10 mo of age showed no obvious abnormalities with the exception of autofluorescent storage material. Peripheral tissues of the *PPT1* and *PPT2* knockout mice were histologically normal, except for focal collections of "foamy" histiocytes in the spleens of some of the PPT1-deficient mice. The storage material was autofluorescent, suggesting that it is associated with the genotype and is not an incidental finding.

Discussion

In the current study, we have shown that deficiency in either of the two lysosomal thioesterases causes a neuronal ceroid lipofuscinosis in mice. The phenotypic similarities are somewhat surprising given that the two genes are only 18% identical and have different substrate specificities.

The PPT1-deficient mouse is a robust model for infantile NCL as 100% of the mice are grossly abnormal neurologically by 8 mo of age. Together with the current study, genetic mouse models (two engineered and two naturally occurring) now exist for four of the eight forms of human NCL (19–23). Of these, the current model is among the most severe, with an onset clearly earlier than the *CLN3* knockout (19, 20), the *nclf* mouse [which likely represents a mouse model for NCL-6 (23)], and the *mnd* mouse [which represents NCL-8, or EPMR (progressive epilepsy with mental retardation) or "Northern" epilepsy] (22). The only possible exception is the *mnd* mouse on the AKR background, which has an onset by 4.5–5 mo and death by 7 mo (24).

Notably, myoclonic seizures were a prominent feature in the PPT1-deficient mouse. Approximately 30 mouse genes are associated with different forms of epilepsy (25). Myoclonic seizures are also an important feature of the cystatin B-deficient mouse (26), which is a model for *EPM1*, or progressive myoclonic epilepsy (Unverricht–Lundborg type) (27). The human disorder *EPM1* shares many of the phenotypic features of the NCLs, and in fact, the NCLs were often classified within the progressive myoclonic epilepsies before the lysosomal nature of NCLs was appreciated. The phenotypic similarities between cystatin B and PPT-deficient mice (and the corresponding human disorders) are sufficiently striking to suggest that a common pathway may be involved. Cystatin B is a cytosolic protein that potently inhibits cathepsins, several of which are lysosomal (28, 29). One postulated function of cystatin B is to inhibit "escaped" lysoso-

mal proteases before they can activate caspases or cause other cell damage (27). It is interesting to note that many of the substances that accumulate in lysosomal storage disorders may have membrane-disruptive, detergent-like properties (the fatty acid thioesters that accumulate in infantile NCL are an excellent example). A parsimonious explanation for the neurodegeneration associated with certain lysosomal storage disorders may be that they allow access of lysosomal proteases to the cytosolic compartment, where the proteases overwhelm the inhibitory machinery of the cytosol. The current study provides tools with which this hypothesis could be addressed.

Of the 50 known lysosomal enzymes, corresponding human disorders exist for ≈40 of them (30). Therefore, it would not be surprising if PPT2 deficiency produces a disorder in humans, as it does in mice. How might PPT2 deficiency be recognized in humans? The current study suggests that PPT2 deficiency would resemble a milder form of NCL. Recently, two sisters with mild PPT1 deficiency were described; these patients suffered from depression and other psychiatric symptoms for a decade (beginning in their thirties), before developing dementia and motor difficulties (31). In these cases, electron microscopy (characteristic "GROD" pathology) led to the diagnosis of PPT1 deficiency. Unfortunately, PPT2-deficient mice at 10 mo of age show no characteristic inclusions in their brains, even though the autofluorescence is striking. In infantile NCL patients, it is sometimes necessary to perform serial biopsies over time to demonstrate GROD pathology (17). It is possible that PPT2-deficient mice will develop GROD or similar material identifiable by electron microscopy as they age.

The phenotype in the PPT2-deficient mice suggests that PPT2 has some unique function that PPT1 cannot carry out. Although both enzymes hydrolyze long chain fatty acyl CoAs with a similar fatty acid chain length optimum of 14–18 carbons, PPT2 hydrolyzes very-long chain fatty acids more efficiently than PPT1 (5, 11, 32). It would be interesting to see whether these fatty acyl CoAs accumulate in the brains of PPT2-deficient mice, which would support a role for PPT2 in their removal.

In conclusion, we have produced knockouts of *PPT1* and *PPT2* genes in mice and shown that both produce a neuronal ceroid lipofuscinosis. The *PPT1* mouse is an excellent model that will provide a substrate for testing therapy. The *PPT2* mouse will provide insights into the function of PPT2 and suggests a phenotype for a possible human disorder.

We thank Elizabeth Lummus, Jeff Stark, and Chris Pomajzl for expert technical assistance. This study was supported by grants from the National Institutes of Health (NS36867 and NS32353), the Batten Disease Support and Research Association, and the Perot Family Foundation.

1. Hofmann, S. L. & Peltonen, L. (2001) in *The Neuronal Ceroid Lipofuscinoses*, eds. Scriver, C. R., Beaudet, A. L., Sly, W. S., Childs, B. & Vogelstein, B. (McGraw–Hill, New York), Vol. 8, pp. 3877–3894.
2. Mole, S. E. (1999) *Lancet* **354,** 443–445.
3. Hofmann, S. L., Das, A. K., Lu, J. Y. & Soyombo, A. A. (2001) *Adv. Genet.* **45,** 69–92.
4. Lu, J. Y., Verkruyse, L. A. & Hofmann, S. L. (1996) *Proc. Natl. Acad. Sci. USA* **93,** 10046–10050.
5. Soyombo, A. A. & Hofmann, S. L. (1997) *J. Biol. Chem.* **272,** 27456–27463.
6. Herz, J., Clouthier, D. E. & Hammer, R. E. (1992) *Cell* **71,** 411–421.
7. Mansour, S. L., Thomas, K. R. & Capecchi, M. R. (1988) *Nature (London)* **336,** 348–352.
8. Rohlmann, A., Gotthardt, M., Willnow, T. E., Hammer, R. E. & Herz, J. (1996) *Nat. Biotechnol.* **14,** 1562–1565.
9. Willnow, T. E. & Herz, J. (1994) *Methods Cell Biol.* **43,** 305–334.
10. Das, A. K., Lu, J. Y. & Hofmann, S. L. (2001) *Hum. Mol. Genet.* **10,** 1431–1439.
11. Camp, L. A., Verkruyse, L. A., Afendis, S. J., Slaughter, C. A. & Hofmann, S. L. (1994) *J. Biol. Chem.* **269,** 23212–23219.
12. Voznyi, Y. V., Keulemans, J. L., Mancini, G. M., Catsman-Berrevoets, C. E., Young, E., Winchester, B., Kleijer, W. J. & van Diggelen, O. P. (1999) *J. Med. Genet.* **36,** 471–474.
13. Martin, J. E. & Shaw, G. (1998) *Neuropathol. Appl. Neurobiol.* **24,** 83–87.
14. Shelton, J. M., Lee, M. H., Richardson, J. A. & Patel, S. B. (2000) *J. Lipid Res.* **41,** 532–537.
15. Salonen, T., Hellsten, E., Horelli-Kuitunen, N., Peltonen, L. & Jalanko, A. (1998) *Genome Res.* **8,** 724–730.
16. Labat-Moleur, F., Guillermet, C., Lorimier, P., Robert, C., Lantuejoul, S., Brambilla, E. & Negoescu, A. (1998) *J. Histochem. Cytochem.* **46,** 327–334.
17. Das, A. K., Becerra, C. H. R., Yi, W., Lu, J.-Y., Siakotos, A. N., Wisniewski, K. E. & Hofmann, S. L. (1998) *J. Clin. Invest.* **102,** 361–370.
18. Soyombo, A. A., Yi, W. & Hofmann, S. L. (1999) *Genomics* **56,** 208–216.
19. Mitchison, H. M., Bernard, D. J., Greene, N. D., Cooper, J. D., Junaid, M. A., Pullarkat, R. K., de Vos, N., Breuning, M. H., Owens, J. W., Mobley, W. C., *et al.* (1999) *Neurobiol. Dis.* **6,** 321–334.
20. Katz, M. L., Shibuya, H., Liu, P. C., Kaur, S., Gao, C. L. & Johnson, G. S. (1999) *J. Neurosci. Res.* **57,** 551–556.
21. Bronson, R. T., Lake, B. D., Cook, S., Taylor, S. & Davisson, M. T. (1993) *Ann. Neurol.* **33,** 381–385.
22. Ranta, S., Zhang, Y., Ross, B., Lonka, L., Takkunen, E., Messer, A., Sharp, J., Wheeler, R., Kusumi, K., Mole, S., *et al.* (1999) *Nat. Genet.* **23,** 233–236.
23. Bronson, R. T., Donahue, L. R., Johnson, K. R., Tanner, A., Lane, P. W. & Faust, J. R. (1998) *Am. J. Med. Genet.* **77,** 289–297.
24. Messer, A., Manley, K. & Plummer, J. A. (1999) *Mol. Genet. Metab.* **66,** 393–397.
25. Puranam, R. S. & McNamara, J. O. (1999) *Curr. Opin. Neurobiol.* **9,** 281–287.
26. Pennacchio, L. A., Bouley, D. M., Higgins, K. M., Scott, M. P., Noebels, J. L. & Myers, R. M. (1998) *Nat. Genet.* **20,** 251–258.
27. Pennacchio, L. A., Lehesjoki, A. E., Stone, N. E., Willour, V. L., Virtaneva, K., Miao, J., D'Amato, E., Ramirez, L., Faham, M., Koskiniemi, M., *et al.* (1996) *Science* **271,** 1731–1734.
28. Turk, V. & Bode, W. (1991) *FEBS Lett.* **285,** 213–219.
29. Barrett, A. J. & Salvesen, G. (1986) *Proteinase Inhibitors* (Elsevier, Amsterdam).
30. Meikle, P. J., Hopwood, J. J., Clague, A. E. & Carey, W. F. (1999) *J. Am. Med. Assoc.* **281,** 249–254.
31. van Diggelen, O. P., Thobois, S., Tilikete, C., Zabot, M. T., Keulemans, J. L., van Bunderen, P. A., Taschner, P. E., Losekoot, M. & Voznyi, Y. V. (2001) *Ann. Neurol.* **50,** 269–272.
32. Aguado, B. & Campbell, R. D. (1999) *Biochem. J.* **341,** 679–689.